Development of Organo-Dispersible Graphene Oxide via Pseudo-Surface Modification for Thermally Conductive Green Polymer Composites

ACS OMEGA

Article

Cite This: ACS Omega 2018, 3, 18124−18131

http://pubs.acs.org/journal/acsodf

Development of Organo-Dispersible Graphene Oxide via Pseudo-Surface Modification for Thermally Conductive Green Polymer Composites

Siewteng Sim,[†] Yoshito Andou,*[,†] Hamra A. A. Bashid,[‡] Hongngee Lim,[‡] Mohammednoor Altarawneh,[§] Zhongtao Jiang,[§] Kubra Eksiler,[†] and Satoshi Iikubo[†]

[†]Department of Biological Functions Engineering, Graduate School of Life Science and Systems Engineering, Kyushu Institute of Technology, 2-4 Hibikino, Wakamatsu-ku, Kitakyushu, Fukuoka 808-0196, Japan

[‡]Department of Chemistry, Faculty of Science, Universiti Putra Malaysia, UPM, Serdang 43400, Selangor, Malaysia

[§]School of Engineering and Information Technology, Murdoch University, 90 South Street, Murdoch, Western Australia 6150, Australia

Supporting Information

ABSTRACT: Graphene has attracted lots of researchers attention because of its remarkable conductivity in both electrically and thermally. However, it has poor dispersibility in organic solvents which limited its applications. Polymers with aromatic end group which act as an intercalator were prepared by ring-opening polymerization with ε-caprolactone by utilizing 1-naphthalene methanol (1-NM) as an initiator. These intercalators will exist between graphene oxide (GO) sheets to prevent aggregation via interactions. The attachment of 1-NM on polymer chains was supported by ultraviolet−visible spectra, size exclusion chromatography profiles, and ^{1}H nuclear magnetic resonance spectra. Exfoliated structured functionalized GO (fGO)/polycaprolactone (PCL) (synthesized fGO) nanocomposites that dispersed well in acetone, chloroform, *N*,*N*-dimethylformamide, dimethyl sulfoxide, tetrahydrofuran, and toluene were successfully synthesized. This agreed well with the enlarged interlayer spacing in the optimized fGO as compared to that of GO from density functional theory simulations using the DMol^3 module that implemented in the Materials Studio 6.0. Furthermore, its potential to be applied as green electronics in electronics, aerospace, and automotive industries was presented, by trailering the thermal conductivity enhancement from the incorporation of fGO/PCL with commercialized biodegradable polymers, PCL, and poly[(*R*)-3-hydroxybutyric acid].

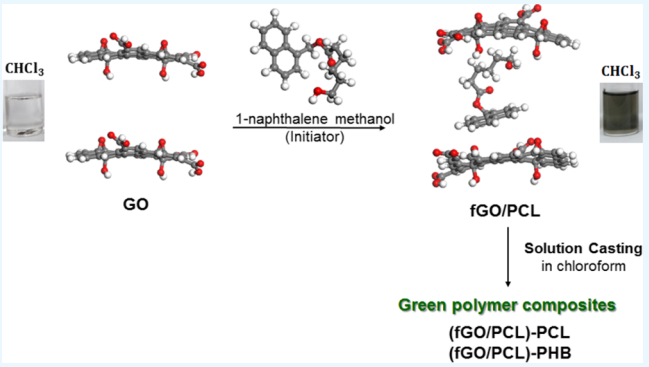

1. INTRODUCTION

The discovery of graphene has sparked the evolution of materials as the most recent superior material in human history. It has atomically thick sp^2-hybridized carbon atoms arranged in a honeycomb structure within a two-dimensional lattice. The unique plane structure and geometry of monolayer graphene contribute to its incredible properties. It is thin flake and lightweight. This material is the strongest material ever measured and possesses Young's modulus of 1 TPa and an ultimate strength of 130 GPa.[1] In addition, it has excellent electrical (∼6000 S/cm)[2] and thermal conductivities (∼5000 W/mK),[3] a large specific surface area (2630 m^2/g), and gas impermeability.[4] Owing to its excellent properties, it can be utilized as conductive ink and/or paste for printed circuits in electronics, sensors, and so forth for internet of things and any subtracts such as clothes, skin, glass, and so forth for various applications.

In this modern era, people are living in a world of electronics, from home and office, to industries, and even outer space. Electronic devices either low-powered or high-powered are consuming power and generating intense heat which causes low performance and efficiency. Additionally, continued miniaturization of electronic devices requires them to be lightweight, efficient heat dissipation, easy to deform, and affordable by customers. Consequently, thermally conductive polymer composites emerged as heat removers in various applications such as heat exchangers, electric generators, power electronics, and so forth.[5] Furthermore, the key prerequisite for achieving sustainability in the electronic industry is the usage of electronic devices that benign integration into life and environment, which are known as green electronics.

Graphene appears to be the most promising candidate for the production of green electronic that possesses various incredible properties especially thermal and electrical con-

Received: September 22, 2018
Accepted: December 7, 2018
Published: December 24, 2018

DOI: 10.1021/acsomega.8b02478
ACS Omega 2018, 3, 18124−18131

ductivities, electromagnetic shielding, and mechanical enhancement, by incorporating it with biodegradable polymers. However, because of the high surface area, van der Waals force, and $\pi-\pi$ interactions of graphene sheets, these multilayered sheets tend to aggregate and cause dispersion problems in various solvents and polymer matrices. The dispersion of fillers within a polymer matrix plays an important role in achieving good properties for the composites.

Hence, surface modification of graphene is crucial to improve its solubility and dispersibility, and these modifications can be performed via covalent and noncovalent methods. Covalent methods involve the addition of organic groups such as amines and polymers via amide or ester bonds on the graphene surface, followed by the transformation of the hybridized atoms from sp^2 to sp^3.[6] Ring-opening polymerization (ROP) of ε-caprolactone (ε-CL) with graphene oxide (GO) as an initiator successfully obtained an exfoliated polycaprolactone (PCL)−GO composites through generation of PCL from hydroxy groups on the surface of GO.[7] However, the main drawback for this modification method is that the aromatic systems of the graphene are disrupted; therefore, the graphene derivatives compromised electrical conductivity and mechanical properties.[8]

Noncovalent methods include $\pi-\pi$ stacking interactions, hydrophobic effects, van der Waals forces, and electrostatic interactions.[6] These noncovalent methods can maximally preserve graphene's original structure, whereas molecules adsorb on its surfaces.[8] Melt processing, solvent processing, and in situ polymerization are the most common methods for preparing graphene nanocomposites with noncovalent interactions.[9] A co-continuous structure was obtained by trapping graphene at the interface of PCL/polylactic acid blend, resulted in improved thermal conductivity and extremely low thermal percolation threshold.[10] Compared to solution mixing methods, a well-dispersed graphene-based filler can be obtained via in situ polymerization without a prior exfoliation step.[11] In situ intercalation polymerization, where the monomer is intercalated between layers of graphene or GO, followed by polymerization to prevent aggregation, has been reported.[12] Jang et al. proposed a novel method to prepare nanocomposites between GO and poly(methyl methacrylate) by utilizing a macro-azoinitiator (MAI).[12] The MAI acted as an intercalator and exfoliated GO. Nanocomposites prepared by this technique have improved in conductivity.

Herein, we report the introduction of dispersible functionalized GO (fGO) through a novel pseudo-surface modification, which known as in situ intercalation polymerization. We demonstrated one of the most common types of polymerization, ROP of ε-CL with 1-naphthalene methanol (1-NM) as an initiator to prepare PCL with aromatic end groups which played as an intercalator. These polymers intercalated between GO sheets via noncovalent interactions to prevent aggregation. The effectiveness of proposed pseudo-modification on the preparation of dispersible fGO in organic solvents and polymer matrixes is investigated both theoretically and experimentally.

2. RESULTS AND DISCUSSION

2.1. Synthesis of PCL in the Presence of 1-Naphthalene Methanol/Tin(II) 2-Ethylhexanoate and Butanol/Tin(II) 2-Ethylhexanoate Catalytic System. It is commonly known that synthesis of PCL via ROP involves an alcohol (R−OH) as an initiator and tin(II) 2-ethylhexanoate, $Sn(Oct)_2$, as a catalyst. In order to confirm PCL generated from hydroxy group of 1-NM on size exclusion chromatography (SEC) measurement, aromatic and aliphatic alcohols were, respectively, used as initiators, 1-NM and butanol, to form PCL in this study. This set of experiments give basic understanding of synthesized PCL with different kinds of initiators. Table 1 shows the similar polydispersity index from both synthesized PCL. The structure of the synthesized PCL was characterized by ^{1}H nuclear magnetic resonance (^{1}H NMR) spectra, as shown in Figure S1. The results clearly indicate that typical ^{1}H NMR chemical shifts at 1.38 ($CH_2CH_2CH_2COO$), 1.64 (CH_2CH_2COO), 2.30 (CH_2COO), 4.06 (CH_2OCO), and 3.65 (CH_2CH) ppm were associated with PCL in both spectra.[13] Incorporation of 1-NM into PCL chains is confirmed with the proton peaks at 5.58 ($C_{10}H_7CH_2OH$) and 7.30−8.00 ($C_{10}H_7CH_2$) ppm which can be observed in Figure S1a.

Table 1. Molecular Weights, Polydispersity Index, and Yield of Synthesized PCL[a]

sample	M_n (g/mol)	M_w (g/mol)	M_w/M_n	yield (%)
PCL (with butanol)	15 000	16 200	1.07	71
PCL (with 1-NM)	17 600	18 700	1.06	77

[a]Reaction conditions: ε-CL 26 mmol; 1-NM and butanol 0.2 mmol; DMF 3 mL; tin(II) 2-ethylhexanoate catalytic amounts; T = 75 °C.

Figure 1 shows the SEC profiles of synthesized PCL (with 1-NM) and PCL (with butanol). However, SEC profiles of both PCL were significantly different. The changes in the UV/RI intensity ratio of each fraction in SEC profiles of the synthesized PCLs, PCL (with 1-NM), and PCL (with butanol) are exhibited in Figure 1. They act as an indicator for the attachment of aromatic hydrocarbon, 1-NM on PCL chain. It was found that there is a high value in the UV/RI ratio value of PCL generated from 1-NM. Figure 1a indicates alike shape and similar average molecular weights of both RI and UV profiles for PCL (with 1-NM). The [1-NM] unit ratio of each fraction in the SEC profile was nearly constant in the range of 0.37−0.44 over the whole peak profile. According to Figure 1b, PCL that synthesized with butanol does not have significant UV profile and any [aromatic] unit ratio because it categorized as a nonaromatic compound. The UV absorption of ε-CL unit is considered to be negligible as compared to that of the 1-NM unit.[14] Therefore, the monitored UV can be interpreted as the distribution of 1-NM unit.

2.2. Mechanism and Theoretical Results of Pseudo-Surface Modification. The first step of the ROP involved the formation of active species ($C_{10}H_7CH_2O-$) by reacting the 1-NM and tin catalyst. Subsequently, the nucleophilic attack of the alkoxide bond of active species on the carbonyl group of ε-CL to obtain PCL with aromatic end groups, which act as an intercalator as shown in Scheme 1a. These polymers intercalated between GO sheets as shown in Scheme 1b via noncovalent interactions to prevent stacking of GO sheets to occur. "Pseudo-surface modification" was inspired by these pretentious and pseudo interactions between GO and intercalator.

From density functional theory (DFT) simulation, the interlayer spacing of optimized fGO simulation cell was 1.33 nm and was slightly larger than that of GO simulation cell, which was 1.10 nm. This result proved the effectiveness of the proposed pseudo-surface modification in preventing aggregation of GO.

DOI: 10.1021/acsomega.8b02478
ACS Omega 2018, 3, 18124−18131

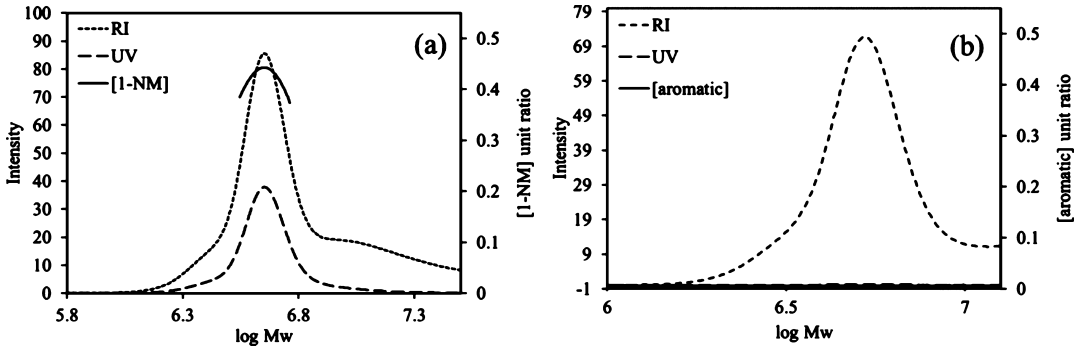

Figure 1. SEC profiles monitored by RI and UV detectors and (a) [1-NM] unit ratio for PCL (with 1-NM); (b) [aromatic] unit ratio for PCL (with butanol).

Scheme 1. (a) Hypothetical Mechanisms of the ROP of ε-CL in the Presence of 1-Naphthalene Methanol/Tin(II) 2-Ethylhexanoate Catalytic System and (b) Route for Synthesis of Intercalated fGO/PCL Nanocomposites

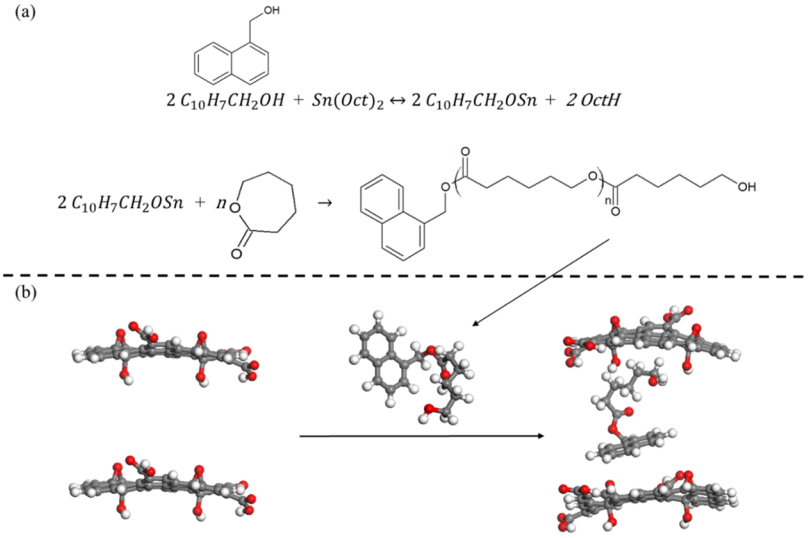

The interaction energy was estimated from the energy difference (ΔE) between the total potential energy of the GO/monomer system and the sum of the potential energies of the individual molecules as shown in the equation below[15]

$$E_{\text{interaction}} = E_{\text{total}} - (E_{\text{GO}} + E_{\text{monomer}})$$

where $E_{\text{interaction}}$ is the interaction potential energy (−8 kcal/mol), E_{total} is the total potential energy of the GO/monomer system (−3 671 390 kcal/mol), E_{GO} is the potential energy of GO (−3 115 116 kcal/mol), and E_{monomer} is the potential energy of ε-CL (−556 266 kcal/mol). The negative value of interaction energy indicated that GO and monomer were attracted to each other.[16] Furthermore, the systems were thermodynamically stable and exothermic.[16]

2.3. Dispersibility of fGO/PCL Nanocomposites in Organic Solvents. fGO/PCL nanocomposites were prepared via ROP in the presence of 1-NM with 5 and 10 mg of GO, which named 0.19 wt % fGO/PCL and 0.36 wt % fGO/PCL, respectively. Tables 1 and 2 indicate the similar polydispersity index from PCL (with 1-NM) and fGO/PCL nanocomposites. Nevertheless, PCL (with 1-NM) presented the highest molecular weights as compared to that of fGO/PCL nanocomposites.

In order to prepare higher molecular weight of fGO/PCL, 0.37 wt % fGO/PCL* was synthesized by using ratio of ε-CL to 1-NM equal to 600 and extended reaction time to 64 h.

Table 2. Results of Molecular Weights, Polydispersity Index, and Yield of fGO/PCL Nanocomposites[a]

sample	M_n (g/mol)	M_w (g/mol)	M_w/M_n	yield (%)
0.19 wt % fGO/PCL	14 900	15 600	1.05	85
0.36 wt % fGO/PCL	11 800	12 600	1.07	90
0.37 wt % fGO/PCL*	10 900	15 900	1.46	88

[a]Reaction conditions: GO 5 mg or 10 mg; ε-CL 26 mmol; 1-NM and butanol 0.2 mmol; DMF 3 mL; tin(II) 2-ethylhexanoate catalytic amounts; T = 75 °C; t = 18 h. Reaction conditions for *: GO 46 mg; ε-CL 120 mmol; 1-NM 0.2 mmol; DMF 4 mL; tin(II) 2-ethylhexanoate catalytic amounts; T = 75 °C; t = 64 h.

As illustrated in Figure 2, both fGO/PCL nanocomposites showed similar trends of the ratio of UV to RI to that of PCL (with 1-NM). This proves the attachment of 1-NM in PCL chains in both nanocomposites. The [1-NM] unit ratios for 0.19 wt % fGO/PCL and 0.36 wt % fGO/PCL were nearly constant in the range of 0.47−0.54 and 0.50−0.58, respectively.

GO readily dissolves in water and some solvents with high boiling point such as dimethylformamide (DMF), dimethyl sulfoxide (DMSO), and *N*-methyl-2-pyrrolidone.[17] However, dispersion in common organic solvents mainly the one with low boiling point such as acetone, chloroform, and tetrahydrofuran (THF) is the most typical problem faced by

DOI: 10.1021/acsomega.8b02478
ACS Omega 2018, 3, 18124−18131

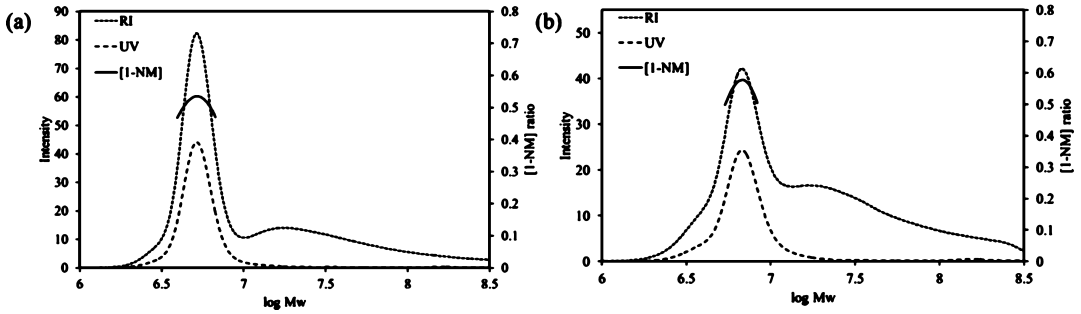

Figure 2. SEC profiles monitored by RI and UV detectors and [1-NM] unit ratio for (a) 0.19 wt % fGO/PCL and (b) 0.36 wt % fGO/PCL.

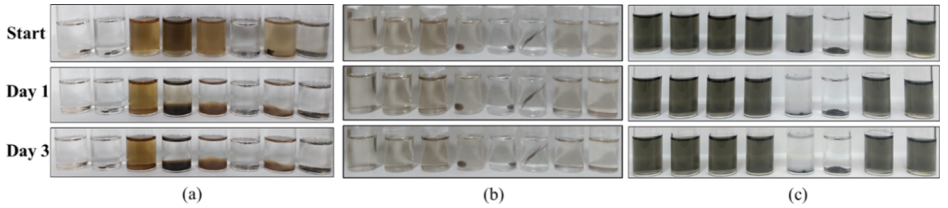

Figure 3. Photograph of (a) GO, (b) standard experiment, 0.36 wt % GO + PCL, and (c) 0.36 wt % fGO/PCL that dispersed in eight organic solvents (from left to right: acetone, chloroform, DMF, DMSO, ethanol, hexane, THF, and toluene) through bath ultrasonication for 2 h. Top: Dispersions immediately after sonication. Middle: Dispersions one day after sonication. Bottom: Dispersions three days after sonication.

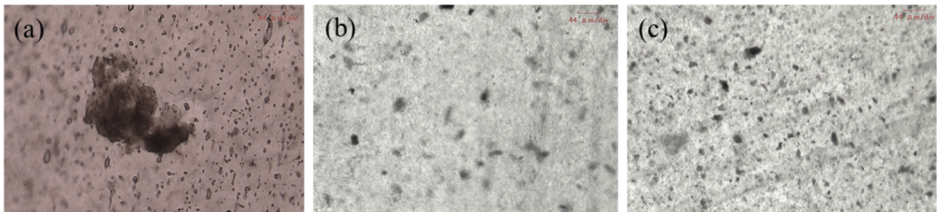

Figure 4. Optical images of (a) standard experiment (0.36 wt % GO in commercialized PCL), (b) 0.19 wt % fGO/PCL and (c) 0.36 wt % fGO/PCL nanocomposite samples with magnification of 1000.

GO. The aggregation of GO sheets and 0.36 wt % GO + PCL (standard experiment) is observed in Figure 3a,b, respectively. GO and 0.36 wt % GO + PCL with concentrations of 0.33 and 8.0 mg mL^{-1}, respectively, only dispersed well in DMF 3 days after sonication. On the other hand, 0.36 wt % fGO/PCL with concentration as high as 8.0 mg mL^{-1} presented outstanding dispersion performance in Figure 3c, where well-dispersed homogeneous dispersion was observed 3 days after sonication in more organic solvents, including the one with low boiling point such as acetone, chloroform, and THF. This experimental test agreed well with the enlarged interlayer spacing in the optimized fGO from theoretical results in Section 2.2. At the same time, optical images reveal the full distribution from fGO/PCL nanocomposites and poor distribution from 0.36 wt % GO + PCL in Figure 4.

Besides visual inspection, UV−visible absorption (UV−vis) spectroscopy was employed to gain further insight into the capability of fGO/PCL nanocomposites to disperse in organic solvents. The UV−vis spectra were obtained under identical conditions (i.e., all samples were obtained after immediate sonication in DMF) and diluted to obtain absorbance value less than one. As presented in Figure 5, a peak at around 270 nm (red arrow) and a shoulder at ∼300 nm were observed in the GO spectrum, which might corresponding to $\pi \rightarrow \pi^*$ transitions of aromatic C−C bonds and $n \rightarrow \pi^*$ transitions of C═O bonds, respectively.[18] PCL shows characteristic peaks similar to that of 1-NM, in the wavelength region shorter than

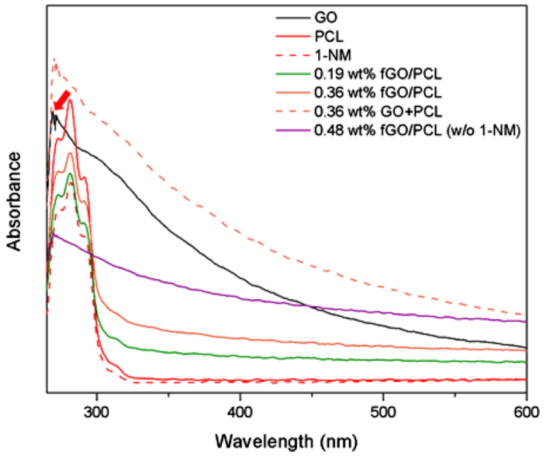

Figure 5. UV−vis absorption spectra for GO, PCL, 1-NM, fGO/PCL nanocomposites, and standard experiments, 0.36 wt % GO + PCL and 0.48 wt % fGO/PCL (w/o 1-NM) in DMF. The spectra were recorded for immediate dispersions after 2 h of bath ultrasonication.

300 nm and a shoulder at ∼300 nm, which attributed to the n $\rightarrow$ π^* transition of ester carbonyl and showed negligible change on irradiation.[19] The standard experiments, 0.36 wt % GO + PCL and 0.48 wt % fGO/PCL (w/o 1-NM), showed the spectrum similar to that of GO. This indicates the minor attachment of PCL on the surface of GO, whereas fGO/PCL nanocomposites show absorption curves with feature charac-

DOI: 10.1021/acsomega.8b02478
ACS Omega 2018, 3, 18124−18131

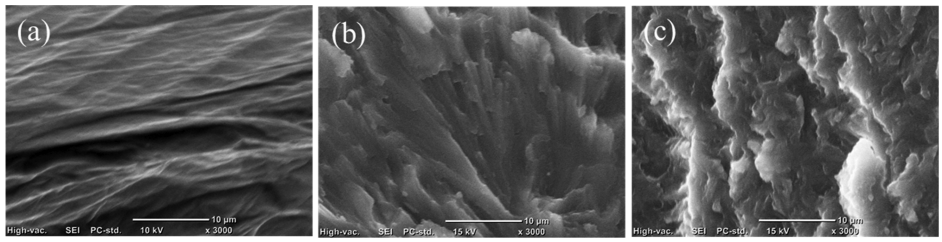

Figure 6. SEM images for (a) GO and fractured structure for (b) PCL and (c) 0.36 wt % fGO/PCL.

teristics for both PCL and GO, indicating their exfoliated structure besides well-dispersed in DMF.

2.4. Characterization of fGO/PCL Nanocomposites. The surface morphology of GO, PCL, and fGO/PCL nanocomposites was studied to consider the distribution and dispersion deeply. Figure 6a,b illustrates the scanning electron microscopy (SEM) images of GO and plain PCL, respectively. Wrinkle surface was observed on GO, whereas smooth and homogeneous surface was observed on fractured PCL. From Figure 6c, a rougher surface compared to plain PCL and without visible aggregation can be observed. It indicates that GO sheets are finely dispersed in the PCL matrix and delamination of GO sheets was effectively induced to yield an exfoliated fGO/PCL nanocomposites. This agreed well with an optical image of 0.36 wt % fGO/PCL in Figure 4c.

The solid-state structure of composite was analyzed by the wide-angle X-ray diffraction (WAXD) pattern, as shown in Figure S2. GO shows a large and broad diffraction peak at about $2\theta = 10.89°$ with the d-spacing 8.12 Å, corresponding to the layered structure of GO.[7] Meanwhile, fGO/PCL nanocomposites showed a typical WAXD pattern of PCL, whereas the peak corresponding to the layered structure of GO was not observed. In results, an exfoliated structure was observed, where the individual GO layers were delaminated and randomly dispersed in the PCL matrix; the distances between the GO layers were too far and the layered were too disordered to give a coherent wide-angle X-ray diffraction (XRD) signal at $2\theta = 2°$.[12]

Fourier transform infrared (FTIR) measurements were carried out to investigate the interactions between GO and PCL, as displayed in Figure S3. A broad band ranged from 3000 to 3700 cm^{-1} indicated the presence of hydroxy groups on GO. The peak at 1640 cm^{-1} was associated with the skeletal vibrations of aromatic C═C bond or intramolecular hydrogen bonds. Other bands at 1100, 1090, and 1050 cm^{-1} correspond to C−O−H deformation, C−H stretching (epoxy groups), and C−O stretching vibrations (alkoxy groups), respectively.[20] The FTIR spectrum of the fGO/PCL nanocomposite was agreed well with that of PCL, where 2950−2860 cm^{-1} indicated C−H hydroxy group stretching; 1700 cm^{-1} indicated −C═O ester carbonyl group stretching; 1240−1178 cm^{-1} indicated C−O−C stretching.[21] The noncovalent interactions between GO and PCL chains proven by the presence of hydroxy groups in PCL and fGO/PCL nanocomposite. The peaks of GO were masked by the peaks of PCL because of relatively less content of GO.

Figure S4 and Table 3 represent the thermal stability of all samples that analyzed by thermogravimetric analysis (TGA). The TGA curve of GO showed two major weight losses. The first weight loss step was started at about 100 °C because of vaporization of water on GO sheets, whereas the second weight loss step was started at approximately 200 °C because of decomposition of oxygen containing functional groups (i.e., C═O, C−O−C, and −OH).[22] The characteristic degradable temperature of PCL was about 120 °C. In general, fGO/PCL nanocomposites showed slightly improved thermal stability as compared to PCL according to the temperature at the 50 and 10% weight losses that stated in Table 3. This result revealed that there was no significant interactions such as covalent interactions among GO and PCL. It complied with the proposed interaction which was noncovalent interactions.

Table 3. Thermal Properties of PCL and fGO/PCL Nanocomposites

	thermal parameters					
run	$T_{50\%}$[a] (°C)	$T_{10\%}$[a] (°C)	T_c[b] (°C)	T_m[b] (°C)	ΔH_m[b] (J/g)	X_c[b] (%)
PCL	317	336	29.4	52.8	85.2	62.6
0.19 wt% fGO/PCL	320	352	33.9	52.7	77.9	57.3
0.36 wt% fGO/PCL	320	357	35.0	52.7	71.0	52.2

[a] $T_{50\%}$, $T_{10\%}$ are temperature of degradation, which are obtained from the TGA curves (Figure S4). [b] T_c is the crystallization temperature, T_m is the melting temperature, and ΔH_m is the enthalpy of fusion, which are obtained from DSC curves (Figure S5).

Figure S5 and Table 3 show the results from differential scanning calorimetry (DSC) curves and detailed thermal parameters of all samples. From Figure S5a, neat PCL showed a wide crystallization peak with a crystallization temperature (T_c) of 29.4 °C. The crystallization peak narrowed and T_c increased moderately upon the incorporation of GO. However, melting temperature (T_m) and enthalpy of fusion (ΔH_m) of fGO/PCL nanocomposites decreased as compared to neat PCL, which indicated that enhancement in crystallization did not occur. In result, degree of crystallinity reduced. This might be due to low volume fraction of GO in PCL matrix that resulted less surface nucleation sites.[23] From the value of ΔH_m, the degree of crystallinity (X_c) can be calculated from the following equation

$$X_c = \frac{\Delta H_m}{\Delta H_m^\circ} \times 100\%$$

where ΔH_m° is the fusion enthalpy of pure crystalline PCL with the value of 136 J/g.[24]

2.5. Dispersibility of fGO/PCL Nanocomposites in Polymer Matrixes. In order to envision the potential of fGO/PCL nanocomposites in electronics, aerospace, and automotive industries by utilizing its improved dispersion properties in polymer matrixes and GOs intrinsic exceptional thermal conductivity, two types of biodegradable polymer-based green polymer composites were prepared. The chosen commercialized biodegradable polymers were PCL and poly[(*R*)-3-hydroxybutyric acid] (PHB). Thermal conductivity was studied in two directions, which were cross-plane (φ_c) and

DOI: 10.1021/acsomega.8b02478
ACS Omega 2018, 3, 18124−18131

Table 4. Comparison of the Cross-Plane, φ_c and In Plane, φ_i Thermal Conductivities Enhancement, φ of (0.37 wt % fGO/PCL*)-PCL and (0.37 wt % fGO/PCL*)-PHB Composites

	thermal conductivity enhancement, φ (%)	
sample	cross-plane, φ_c	in-plane, φ_i
(0.37 wt % fGO/PCL*)-PCL	29	72
(0.37 wt % fGO/PCL*)-PHB	9	38

in-plane (φ_i), as shown in Table 4. In cross-plane direction, the obtained thermal conductivities of commercialized PCL and PHB were 0.21 and 0.20 W/m·K, respectively, whereas in in-plane direction, 0.29 and 0.37 W/m·K were gained for commercialized PCL and PHB, respectively.

In general, PCL-based green polymer composite (0.37 wt % fGO/PCL*)-PCL showed more satisfying thermal conductivity enhancement in both direction as compared to that of PHB-based green polymer composite (0.37 wt % fGO/PCL*)-PHB. This was believed due to better dispersion of fGO/PCL* nanocomposite in the PCL matrix. Apart from that, there is a noticeable thermal conductivity enhancement in in-plane for both green polymer composites. In-plane thermal conductivity enhancement (72 and 38%) was revealed for (0.37 wt % fGO/PCL*)-PCL and (0.37 wt % fGO/PCL*)-PHB, respectively. Figure S6 reveals good dispersion of intercalated fGO/PCL* nanocomposite in polymer matrices, which promotes the formation of continuous pathways by improving the direct contact between each nanocomposite resulted low thermal percolation threshold in in-plane direction. The cross-plane thermal conductivity enhancement for (0.37 wt % fGO/PCL*)-PCL and (0.37 wt % fGO/PCL*)-PHB was 29 and 9%, respectively. The slight enhancement in thermal conductivity can be explained by weak noncovalent bonding such as van der Waals force with adjacent unhybridized GO orbitals lying perpendicular to the plane.[25]

3. CONCLUSIONS

In summary, a facile and novel pseudo-surface modification method, which is known as in situ intercalation polymerization by demonstrating ROP with ε-CL with 1-NM as an initiator to prepare an organo-dispersible GO, was reported. Results from UV−vis spectra, SEC profiles, and ^{1}H NMR spectra reveal the attachment of aromatic hydrocarbon, 1-NM on an intercalator. fGO/PCL showed excellent dispersion performance that agreed well with the enlarged interlayer spacing in the optimized fGO from DFT simulations. To confirm the mechanism of proposed pseudo-surface modification, standard experiment was prepared by suspending GO with commercialized PCL in chloroform, which known as GO + PCL. According to dispersion test, optical images, and UV−vis, an exfoliated structured organo-dispersible fGO/PCL nanocomposite was successfully synthesized. Therefore, its greater thermal conductivity enhancement resulted good distribution in polymer matrixes envisioned the possibility for the application in electronics, aerospace, and automotive industries as green electronics. We can conclude that this method paves the way for the production of dispersible GO in various solvents, and it might be applicable in anionic ring-opening polymerization by introducing other monomers to replace ε-CL.

4. EXPERIMENTAL AND COMPUTATIONAL PROCEDURES

4.1. Materials. GO prepared by the modified Hummer's method[26] was supplied by GO Advanced Solutions Sdn. Bhd. (Selangor, Malaysia) and was vacuum-dried before use. The ε-CL (>99%) and 1-NM (>95%) were purchased from TCI (Tokyo, Japan) and were used as received. The acetone (>99.5%), chloroform (>99%), THF (>99.5%), DMSO (>99%), toluene (>99.5%), ethanol (>99.5%), hexane (>96%), butanol (>99%), *N*,*N*-DMF (>99.5%), and tin(II) 2-ethylhexanoate were purchased from Wako Pure Chemical (Japan) and were used as received. PCL (M_n = 80 000) and poly [(*R*)-3-hydroxybutyric acid] were purchased from Sigma-Aldrich and were used as received.

4.2. Sample Preparation. The polymerization of ε-CL was carried out via the ROP with the 1-NM or butanol as initiators to yield PCL (with 1-NM) or PCL (with butanol). The ROP was catalyzed by tin(II) 2-ethylhexanoate. The desired amount of dry GO (5 mg, 10 mg) and 1-NM (31.64 mg, 0.2 mmol) or butanol (14.82 mg, 0.2 mmol) was suspended in ε-CL (2.97 g, 26 mmol) and 3 mL of *N*,*N*-DMF by sonicating for 2 h. Then, the suspension including GO, catalytic amount of tin(II) 2-ethylhexanoate, and ε-CL was transferred to a round bottom flask and sealed with a three-way cock. The flask was degassed by three freeze−pump−thawing cycles and sealed under nitrogen gas conditions. The ROP was carried out at 75 °C for 18 h under vigorous stirring conditions. The resulting solution was precipitated with ethanol, and the obtained product which named fGO/PCL nanocomposite was dried in the vacuum desiccator overnight. The fGO/PCL* nanocomposite was synthesized by using the ratio of ε-CL to 1-NM equal to 600 and 64 h reaction time.

The weight percentage of GO loading was calculated by the following equation:

$$\text{Weight percentage, wt (\%)} = \frac{\text{mass}_{GO}}{\text{mass}_{fGO/PCL}} \times 100\%$$

where mass_{GO} and $\text{mass}_{fGO/PCL}$ are the mass of GO and fGO/PCL nanocomposite, respectively.

4.3. Standard Sample Preparation. In order to confirm the interaction between GO surface and PCL chains, two standard experiments were conducted. GO + PCL (0.36 wt %) was prepared by dispersing 0.36 wt % GO and commercialized PCL in DMF via ultrasonication. On the other hand, 0.48 wt % fGO/PCL (w/o 1-NM) was prepared via ROP in the presence of 10 mg of GO, 2.97 g of ε-CL, 3 mL of DMF, catalytic amount of tin(II) 2-ethylhexanoate and without 1-NM for 18 h.

4.4. Green Polymer Composite Preparation. Green polymer composites were prepared by suspending 1.2 g of synthesized 0.37 wt % fGO/PCL* and 0.3 g of biodegradable polymers in chloroform by sonicating for an hour. The chosen polymer matrixes were commercialized PCL and PHB. After that, the suspension was transferred to a Petri dish and placed inside fume hood for film formation. Before compression molding, the film was dried in the vacuum desiccator overnight. At last, the film was prepared by using a hot-press (IMC-180 °C, Imoto Machinery Co., Japan) at 65 °C for 2 min under a pressure of 30 MPa and were labeled as (0.37 wt % fGO/PCL*)-PCL and (0.37 wt % fGO/PCL*)-PHB.

DOI: 10.1021/acsomega.8b02478
ACS Omega 2018, 3, 18124−18131

4.5. Characterizations. The number of average molecular weight (M_n), weight of average molecular weight (M_w), and polydispersity index (M_w/M_n) of PCL and fGO/PCL nanocomposites were measured at 40 °C with a SEC (EcoSEC HLC-8320GPC, TOSOH, Japan) system that equipped with a TSKgel Super HM-M linear column and a refractive detector, using chloroform as an eluent (0.6 mL/min). The molecular mass scale was calibrated with polystyrene standards. The nanocomposite was dissolved in chloroform, and the solution was filtered with a 0.45 μm membrane filter before measurements. EcoSEC-WS software was used to perform calculations.

^{1}H NMR spectra were run to determine the attachment of 1-NM on PCL chain in deuterated chloroform ($CDCl_3$) on a NMR spectrometer (JNM-ECP 500 MHz, JEOL, Japan).

The FTIR spectra were recorded using potassium bromide (KBr) pellets on a FTIR spectrometer (Nicolet iS10, Thermo Scientific, Japan) with the wavenumber range of 400−4000 cm^{-1} by 16 scans at a resolution of 4 cm^{-1}. The UV−visible absorption spectra were recorded on a UV−vis spectrometer (USB 4000, Ocean Optics, Japan) at room temperature. The WAXD measurements were performed using an X-ray diffractometer (MiniFlex 600, Rigaku Co., Japan) at 40 kV and 15 mA at room temperature. Cu Kα radiation (λ = 1.54 Å) was used as the X-ray source. The diffraction angle was scanned from 3° to 70° at a rate of 10°/min.

The thermal properties of PCL and the nanocomposites were characterized by TGA and DSC. TGA was carried out on EXSTAR TG/DTA 6200 (SII Nanotechnology Inc., Japan). The samples were scanned from to 550 °C with the heating rate of 10 °C/min in the protection of nitrogen flow of 100 mL/min. DSC was carried out with EXSTAR DSC 6220 (SII Nanotechnology Inc., Japan). The samples were analyzed in a heat-cool-heat made with the rate of 10 °C/min. Temperature scan was performed in the range of 0−100 °C in a continuous nitrogen flow.

Surface morphologies of PCL and fGO/CPL nanocomposites were observed by a SEM (JCM-6000, JEOL, Japan). The composites samples were prepared by coating with carbon prior to SEM observation. The distribution of GO in matrix was evaluated by an optical microscope (VH-Z500, KEYENCE, Japan) at room temperature.

The cross-plane and in-plane thermal conductivities of polymer composites were measured at room temperature using Hioki Heat Flow Logger LR8432 by the steady-state method.[27] For these measurements, hot-pressed samples with 2 cm × 2 cm and 2 cm × 3 cm were prepared for cross-plane and in-plane thermal conductivity measurements, respectively. The degree of enhancement of thermal conductivity of polymer composite known as thermal conductivity enhancement can be defined as below

$$\varphi = \frac{k_{com} - k_{poly}}{k_{poly}} \times 100\%$$

where k_{com} and k_{poly} represent the thermal conductivity of polymer composite and pristine polymer matrix, respectively.

4.6. Computational Models. In this work, all molecular models were built by using the 3D atomistic tool from Material Studio 6.0. One repeat unit of ring-opened ε-CL that covalently bonded with 1-NM was selected as a polymer material. The polymer dimensions were set as 1 nm × 1 nm, as shown in Figure 7a. A bilayer GO simulation cell (Figure 7b) with 150 atoms was created with slab dimensions of 2 × 2 × 2 nm and angles $\alpha = \beta = \gamma = 90°$. The interlayer spacing of GO sheets was 1.1 nm. GO sheets were formed using the hydroxy and epoxide groups that randomly decorated the graphene surfaces.[28] Carboxylic acid performed this function at the edges of the graphene sheets.[28] fGO simulation cell (Figure 7c) with 190 atoms was created with slab dimensions of 2 × 2 × 2 nm and angles $\alpha = \beta = \gamma = 90°$.

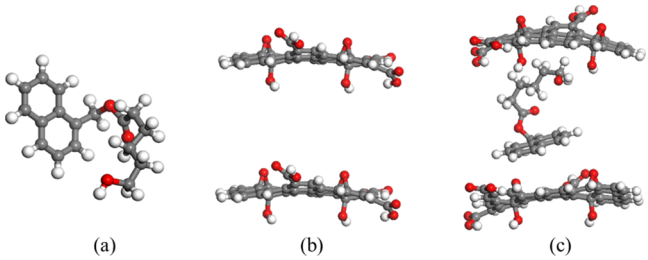

Figure 7. (a) Top view of polymer material; side view of (a) bilayer GO and (c) fGO. Each sphere represents an atom using the following color rule: white, hydrogen; red, oxygen; and gray, carbon.

4.7. Simulation Details. DFT calculations were performed to optimize the structure of models using the DMol^3 module implemented in the Materials Studio 6.0 software package.[29] The PW91 version of the general gradient approximation was combined with a double numerical basis set with *d* polarization (DND) in the calculations. Values of 0.002 Ha for total energy, 0.02 Ha $Å^{-1}$ for force, 0.05 Å for displacement, and 1 × 10^{-5} Ha for the self-consistent field (SCF) computation criterion were chosen to optimize the structures. The direct inversion of the iterative subspace with a subspace size of 10 was used to increase the speed of SCF convergence in these systems. In addition, thermal smearing of the orbital occupation with a smearing of 0.3 Ha was used to increase the speed of SCF convergence in these systems. These parameters have been successfully used to optimize the geometry of the investigated structures.

■ ASSOCIATED CONTENT

Supporting Information

The Supporting Information is available free of charge on the ACS Publications website at DOI: 10.1021/acsomega.8b02478.

^{1}H NMR spectra for PCL with 1-NM and with butanol, WAXD patterns of GO, PCL, and fGO/PCL nanocomposites, FTIR spectra of GO, PCL, and fGO/PCL nanocomposites, TG curves for GO, PCL, and fGO/PCL nanocomposites, DSC curves for GO, PCL, and fGO/PCL nanocomposites during the cooling scan and the second heating scan, and optical images of green polymer composites (0.37 wt % fGO/PCL*)-PCL and (0.37 wt % fGO/PCL*)-PHB with magnification of 2000 (PDF)

■ AUTHOR INFORMATION

Corresponding Author

*E-mail: yando@life.kyutech.ac.jp. Phone: +81-93-884-3672. Fax: +81-93-881-6207 (Y.A.).

ORCID

Yoshito Andou: 0000-0003-3839-0705
Hongngee Lim: 0000-0003-2436-8953
Mohammednoor Altarawneh: 0000-0002-2832-3886

DOI: 10.1021/acsomega.8b02478
ACS Omega 2018, 3, 18124−18131

Zhongtao Jiang: 0000-0002-4221-6841
Satoshi Iikubo: 0000-0002-5186-4058

Author Contributions

The manuscript was written through the contributions of all authors. All authors have given approval to the final version of the manuscript.

Notes

The authors declare no competing financial interest.

REFERENCES

(1) Lee, C.; Wei, X.; Kysar, J. W.; Hone, J. Measurement of the elastic properties and intrinsic strength of monolayer graphene. *Science* **2008**, *321*, 385−388.
(2) Du, X.; Skachko, I.; Barker, A.; Andrei, E. Y. Approaching ballistic transport in suspended graphene. *Nat. Nanotechnol.* **2008**, *3*, 491−495.
(3) Balandin, A. A.; Ghosh, S.; Bao, W.; Calizo, I.; Teweldebrhan, D.; Miao, F.; Lau, C. N. Superior thermal conductivity of single-layer graphene. *Nano Lett.* **2008**, *8*, 902−907.
(4) Bunch, J. S.; Verbridge, S. S.; Alden, J. S.; van der Zande, A. M.; Parpia, J. M.; Craighead, H. G.; McEuen, P. L. Impermeable atomic membranes from graphene sheets. *Nano Lett.* **2008**, *8*, 2458−2462.
(5) Han, Z.; Fina, A. Thermal conductivity of carbon nanotubes and their polymer nanocomposites: A review. *Prog. Polym. Sci.* **2011**, *36*, 914−944.
(6) Georgakilas, V. *Functionalization of Graphene*; Wiley-VCH: Weinheim, 2014; p 110.
(7) Hua, L.; Kai, W.; Inoue, Y. Synthesis and characterization of poly(ε-caprolactone)-graphite oxide composites. *J. Appl. Polym. Sci.* **2007**, *106*, 1880−1884.
(8) Ji, X.; Xu, Y.; Zhang, W.; Cui, L.; Liu, J. Review of functionalization, structure and properties of graphene/polymer composite fibers. *Composites, Part A* **2016**, *87*, 29−45.
(9) Verdejo, R.; Bernal, M. M.; Romasanta, L. J.; Lopez-Manchado, M. A. graphene filled polymer nanocomposites. *J. Mater. Chem.* **2011**, *21*, 3301−3310.
(10) Huang, J.; Zhu, Y.; Xu, L.; Chen, J.; Jiang, W.; Nie, X. Massive enhancement in the thermal conductivity of polymer composites by trapping graphene at the interface of a polymer blend. *Compos. Sci. Technol.* **2016**, *129*, 160−165.
(11) Potts, J. R.; Dreyer, D. R.; Bielawski, C. W.; Ruoff, R. S. Graphene-based polymer nanocomposites. *Polymer* **2011**, *52*, 5−25.
(12) Jang, J.; Kim, M.; Jeong, H.; Shin, C. graphite oxide/poly(methyl methacrylate) nanocomposites prepared by a novel method utilizing macroazoinitiator. *Compos. Sci. Technol.* **2009**, *69*, 186−191.
(13) Sobczak, M. Ring-opening polymerization of cyclic esters in the presence of choline/SnOct2 catalytic system. *Polym. Bull.* **2011**, *68*, 2219−2228.
(14) Yasutake, M.; Hiki, S.; Andou, Y.; Nishida, H.; Endo, T. Physically controlled radical polymerization of vaporized vinyl monomers on surfaces. Synthesis of block copolymers of methyl methacrylate and styrene with a conventional free radical initiator. *Macromolecules* **2003**, *36*, 5974−5981.
(15) Melro, L.; Pyrz, R.; Jensen, L. A molecular dynamics study on the interaction between epoxy and functionalized graphene sheets. *IOP Conf. Ser.: Mater. Sci. Eng.* **2016**, *139*, 012036.
(16) Jia, H.; Su, X.; Hou, G.; Ma, F.; Bi, S.; Liu, Z. Molecular dynamics simulation of interactions on graphene/polypyrrole nanocomposites interface. *Integr. Ferroelectr.* **2013**, *145*, 130−139.
(17) Hernandez, Y.; Lotya, M.; Rickard, D.; Bergin, S. D.; Coleman, J. N. Measurement of multicomponent solubility parameters for graphene facilitates solvent discovery. *Langmuir* **2010**, *26*, 3208−3213.
(18) Paredes, J. I.; Villar-Rodil, S.; Martínez-Alonso, A.; Tascón, J. M. D. Graphene oxide dispersions in organic solvents. *Langmuir* **2008**, *24*, 10560−10564.
(19) Martins-Franchetti, S. M.; Campos, A.; Egerton, T. A.; White, J. R. Structural and morphological changes in poly(caprolactone)/poly(vinyl chloride) blends caused by UV irradiation. *J. Mater. Sci.* **2007**, *43*, 1063−1069.
(20) Shao, W.; Liu, X.; Min, H.; Dong, G.; Feng, Q.; Zuo, S. Preparation, characterization, and antibacterial activity of silver nanoparticle-decorated graphene oxide nanocomposite. *ACS Appl. Mater. Interfaces* **2015**, *7*, 6966−6973.
(21) Abderrahim, B.; Abderrahman, E.; Mohamed, A.; Fatima, T.; Abdesselam, T.; Krim, Q. Kinetic thermal degradation of cellulose, polybutylene succinate and a green composite: Comparative study. *World J. Environ. Eng.* **2015**, *3*, 95−110.
(22) Dehghanzad, B.; Razavi Aghjeh, M. K.; Rafeie, O.; Tavakoli, A.; Jameie Oskooie, A. Synthesis and characterization of graphene and functionalized graphene via chemical and thermal treatment methods. *RSC Adv.* **2016**, *6*, 3578−3585.
(23) Lv, Q.; Wu, D.; Qiu, Y.; Chen, J.; Yao, X.; Ding, K.; Wei, N. Crystallization of Poly(ϵ-caprolactone) composites with graphite nanoplatelets: Relations between nucleation and platelet thickness. *Thermochim. Acta* **2015**, *612*, 25−33.
(24) Tiptipakorn, S.; Keungputpong, N.; Phothiphiphit, S.; Rimdusit, S. Effects of polycaprolactone molecular weights on thermal and mechanical properties of polybenzoxazine. *J. Appl. Polym. Sci.* **2015**, *132*, 41915.
(25) Diaz-Chacon, L.; Metz, R.; Dieudonné, P.; Bantignies, J. L.; Tahir, S.; Hassanzadeh, M.; Sosa, E.; Atencio, R. Graphite nanoplatelets composite materials: Role of the epoxy-system in the thermal conductivity. *J. Mater. Sci. Chem. Eng.* **2015**, *03*, 75−87.
(26) Ng, C. H.; Lim, H. N.; Lim, Y. S.; Chee, W. K.; Huang, N. M. Fabrication of flexible polypyrrole/graphene oxide/manganese oxide supercapacitor. *Int. J. Energy Res.* **2014**, *39*, 344−355.
(27) Zhao, D.; Qian, X.; Gu, X.; Jajja, S.; Yang, R. Measurement techniques for thermal conductivity and interfacial thermal conductance of bulk and thin film materials. *J. Electron. Packag.* **2016**, *138*, 040802.
(28) Mahdavi, M.; Rahmani, F.; Nouranian, S. Molecular simulation of pH-dependent diffusion, loading, and release of doxorubicin in graphene and graphene oxide drug delivery systems. *J. Mater. Chem. B* **2016**, *4*, 7441−7451.
(29) Wang, Y.; Yang, Q.; Li, J.; Yang, J.; Zhong, C. Exploration of nanoporous graphene membranes for the separation of N2 from CO2: a multi-scale computational study. *Phys. Chem. Chem. Phys.* **2016**, *18*, 8352−8358.

DOI: 10.1021/acsomega.8b02478
ACS Omega 2018, 3, 18124−18131